A Comparison of Grid-type Map-building Techniques by Index of Performance

U. Raschke, Student Member, IEEE and **J. Borenstein**, Member, IEEE
The University of Michigan
Advanced Technology Laboratories
1101 Beal Ave., Ann Arbor, MI 48109

This work was sponsored by the Department of Energy Grant DEFG02-86NE37969

Abstract

Grid-type representations for sensor based map-building are becoming increasingly popular in mobile robot applications. Grid-type maps are advantageous because they are computationally easy to maintain, allow for integration of data from different sensors, and can be used to statistically express the confidence in the correctness of the data.

This paper introduces an *index of performance* (IOP), designed to quantitatively express the match between a sensor-built map and a precisely measured reference map. The IOP computes a single value representing the correlation between the sensed object positions in the grid and the actual object positions. With the IOP it is easy to compare the accuracy of different map building methods, as well as the effect of different parameters within a certain method.

Two grid-type map-building algorithms were compared by means of the proposed IOP. One algorithm takes panoramic "snapshots" while the mobile robot is standing, and then uses a probabilistic distribution to update the grid. The other algorithm, called Histogramic In-Motion Mapping (HIMM), is based on rapid sampling of the sensors during motion.

1. Introduction

Mobile robotics research faces the task of building accurate environmental maps from information produced by onboard sensors. Ultrasonic sensors are usually used for this task [1], [2], [3], [7], [8], [9], [10], [12], [13], [15] sometimes in combination with infrared sensors [11] or laser range finders [16]. Ultrasonic sensors are widely available, inexpensive, and easy to control. However, sonar range measurements suffer from fundamental drawbacks that limit their straightforward utilization in mapping applications [2]. The foremost problems are: a) Poor directionality; b) frequent misreadings; and c) specular reflections.

In order to produce useful maps from ultrasonic data, the map-building algorithm must compensate for these shortcomings. Based on the form of data representation, two approaches can be distinguished. a) line-type world models [2], [10], [18]; and b) grid-type world models (GTWMs) [1], [3], [5], [6], [14], [15]. We have extensively experimented with both types of world models and found that GTWMs are more suitable to cope with the problems of ultrasonic sensors; mostly because they allow for a statistical expression of confidence in the correctness of the data.

To improve the quality of map-building, a tool is needed to compare map-building results produced by different methods or different sets of parameters. This paper introduces an *index of performance* (IOP) designed to quantitatively express the match between a sensor-built map and a precisely measured reference map. The proposed IOP is insensitive to grid cell size and therefore allows comparison of algorithms developed with different grid formats. To demonstrate the versatility of the IOP, we present results from application of the IOP to two different map-building methods.

The proposed IOP is described in Section 3, and experimental results and comparisons are given in Section 4.

2. Map Building Methods

2.1 Heuristic Probability Function Mapping

A powerful probabilistic GTWM has been developed at Carnegie Mellon University (CMU) [14],[15]. In this GTWM, the robot work area is represented by a two-dimensional array (certainty grid) of square elements (cells). Each cell contains a certainty value (CV) that indicates the measure of confidence that an obstacle exists within the cell area. CVs are updated by a heuristic probability function (HPF) that takes into account the characteristics of a given sensor. For example, ultrasonic sensors have a conical field of view. A typical ultrasonic sensor [17] returns a radial measure of the distance to the nearest object within the cone, yet does not specify the angular location of the object. Thus, a distance measurement *d* results from an object located anywhere within the area *A* (see Fig. 1). However, an object located near the acoustic axis (the center of the cone) is more likely to produce an echo than an object further away from the acoustic axis [2].

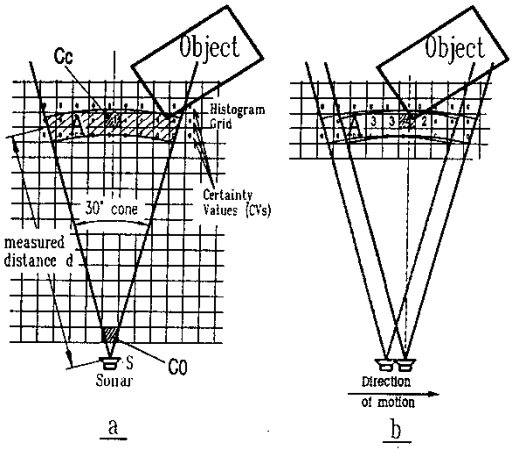

Fig 1.
a) Only a single cell is incremented for each range reading.
b) Histogramic probability distribution obtained by continuous and rapid sampling while the vehicle is moving.

With CMU's certainty grid method, the mobile robot remains stationary while taking a panoramic scan with its ring of 24 ultrasonic sensors. Next, the certainty grid is updated with a probabilistic function C_x that is applied to each one of the 24 range readings. Finally, the robot moves to a new location, stops, and the procedure repeats. After the robot traverses a room in this manner, the resulting certainty grid represents a fairly accurate map of the room.

Additional information can be derived from a range reading concerning the sector between *S* and *A* (see Fig. 1). If an echo is received from an object at distance *d*, then this sector is likely to be free of objects. In [14] this is expressed by applying a probability function with negative values to the cells in the empty area.

The HPF method uses the following distribution functions [14]:

Given the following definitions:

R - the range measurement returned by the sonar sensor,
ε - the mean sonar deviation error,
ω - the beam aperture (angle of cone in Fig. 1a),
δ - the distance between a given cell in the cone and the sensor,
θ - the angle between the acoustic axis of the beam and the axis from the sensor to a given cell in the cone.

The probability that a cell within the sonar cone is empty is given by:

$$p_E(x,y,z) = p[\text{ position}(x,y,z) \text{ is empty}] \quad (1)$$
$$p_E(x,y,z) = E_r(\delta)E_a(\theta)$$

where:

$$E_r(\delta)=1-((\delta - R_{min})/(R - \varepsilon - R_{min}))^2 \text{ for } \delta \in [R_{min}, R - \varepsilon]$$
$$E_r(\delta)= 0 \quad \text{otherwise.} \quad (2)$$

And:

$$E_a(\theta) = 1-(2\theta/\omega)^2 \text{ for } \theta \in [-\omega/2,\omega/2] \quad (3)$$

The probability that a certain cell within the sonar area is occupied is given by:

$$p_O(x,y,z) = p[\text{ position}(x,y,z) \text{ is occupied}] \quad (4)$$
$$p_O(x,y,z) = O_r(\delta)O_a(\theta)$$

where:

$$O_r(\delta)= 1-((\delta - R) / \varepsilon)^2 \text{ for } \delta \in [R - \varepsilon, R + \varepsilon] \quad (5)$$
$$O_r(\delta)=0 \quad \text{otherwise.}$$

And:

$$O_a(\theta) = 1-(2\theta/\omega)^2 \text{ for } \theta \in [-\omega/2,\omega/2] \quad (6)$$

Both occupied cells and empty cells in the certainty grid are updated using probability addition formulas. After a run has been completed, these two types of cells are combined into a final sensor grid. The combination is a thresholding procedure as follows:

Sensor Grid[X,Y] =

$$Occ(X,Y) \quad \text{if } Occ(X,Y) \geq Emp(X,Y) \quad (7)$$
or
$$-Emp(X,Y) \quad \text{if } Occ(X,Y) < Emp(X,Y) \quad (8)$$

The resulting HPF sensor grid contains probabilities ranging from -1 to 1. Values of zero on the HPF grid indicate that no sensor information was obtained for these cells.

2.2 Histogramic In-Motion Mapping

A new method for real-time map building with a mobile robot in motion was recently developed at the University of Michigan [4]. This method, entitled Histogramic In-Motion Mapping (HIMM) uses a two-dimensional Cartesian *histogram grid* for obstacle representation. This representation has been derived from the certainty grid concept described in Section 2.1. Like the certainty grid, each cell in the histogram grid holds a certainty value (CV) that represents the confidence of the algorithm in the existence of an obstacle at that location. The histogram grid differs from the certainty grid in the way it is built and updated. CMU's method projects a probability profile onto *all* those cells affected by a range reading. This procedure is computationally intensive and would impose a heavy time-penalty for real-time execution by a controlling computer. The HIMM method, on the other hand, increments only one cell in the grid for each range reading. For ultrasonic sensors, this cell corresponds to the measured distance *d* and lies on the acoustic axis of the sensor (cell C_c in Fig 1a). While this approach may seem to be an oversimplification, a probabilistic distribution is actually obtained by continuously and rapidly sampling each sensor while the vehicle is moving. The result is a histogramic probability distribution in which high certainty values are obtained in cells close to the actual location of the obstacle (Fig 1b).

The HIMM method also uses the information gained from a sensor reading to update cells in the "empty sector" (between *S* and *A* of Fig. 1a), as does CMU's certainty grid method. However, instead of indicating the absence of objects in this region by computing and projecting a negative probability function for all cells in the sector, the fast sampling approach is used and only those cells that are located on the acoustic axis are decremented.

A final note concerns the actual implementation of HIMM: Whenever a cell is incremented, the increment (denoted I^+) is actually 3 (not 1, as may be expected) and the maximum CV of a cell is limited to $CV_{max} = 15$. Decrements (denoted I^-), however, take place in steps of -1 and the minimum value is $CV_{min} = 0$. Increments are larger than decrements because only one cell is incremented for each reading, whereas multiple cells are decremented (i.e., all cells between C_c and C_o, in Fig. 1a).

3. The Index of Performance

The proposed *index of performance* (IOP) computes a correlation between the sensed position of objects, as computed by the map-building algorithm, and the actual position of the objects, as measured manually.

To enter the actual object positions into the computer, the absolute coordinates of the corners comprising each object are

measured. The lines connecting these coordinates are computed and projected onto a blank grid. In the resulting *actual position grid* (APG), cells are either '1' (filled), if they correspond to the edge of an obstacle, or '0' (empty), if they are inside or outside of an obstacle. Fig. 2 shows typical APGs. Since the resolution of an individual grid cell is on the order of a few centimeters (we use square cells of 10cm sidelength) the reference measurement can be made with an ordinary tape measure.

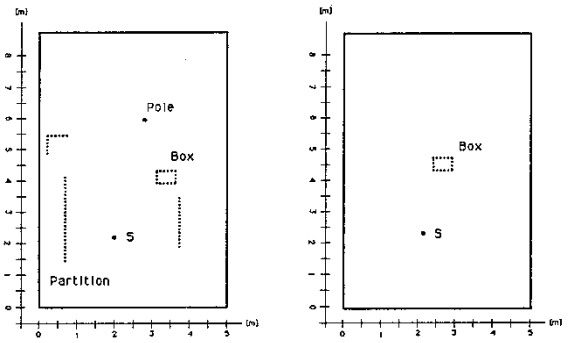

Fig 2. Test obstacle environments.

After this preparation, the robot is run through the obstacle course and a *sensor grid map* is built from sensor data. For each filled cell (i,j) in the sensor grid, the distance to the nearest filled cell in the APG is computed. We denote this distance $D(i,j)_{min}$. Summing $D(i,j)_{min}$ for all filled cells yields a measure of overall accuracy of the system. This method can be refined by weighting each $D(i,j)_{min}$ with its associated certainty value (CV). This is desirable since the CV of a cell is directly related to the count of recurring range readings for the same cell. The IOP can be normalized by dividing the weighted sum of minimum distances by the sum of all CVs. This way, the IOP is independent of the range of CVs of the particular method. The IOP is thus:

$$I = \frac{\sum\left(D_{min}(i,j) * CV_{(i,j)}\right)}{\sum CV_{(i,j)}} \qquad (9)$$

where:

- $D_{min}(i,j)$ - Distance from sensor grid cell (i,j) to the nearest filled cell in the actual position grid (APG).
- $CV_{(i,j)}$ - Certainty value of cell (i,j) in the sensor grid.
- I - Index of Performance.

Statistically, our proposed IOP is analogous to a mean standard deviation calculation. The same type of computation using the more popular statistical variance measure would use a squared distance term $(D(i,j)_{min})^2$. We have chosen to use the unsquared distance term in order to reduce the algorithm's sensitivity to false readings (uncorrelated readings due to noise and crosstalk) that show at random locations in the grid. Also, the IOP based on unsquared terms has the intuitive physical meaning of the *average of all* $D(i,j)_{min}$.

4. Experimental Results

4.1 Test System Configuration

Our experiments were conducted on a Cybermation K2A robot (CYBERMATION) fitted with a ring of 24 ultrasonic sensors. Sensor information was evaluated on a 20 MHz IBM-AT compatible 80386 computer.

Two different map building methods were chosen to demonstrate the versatility of the Index of Performance: our Histogramic In-Motion Mapping algorithm (HIMM), and a heuristic probability function (HPF), similar to the one developed at CMU [14]. The two algorithms (HIMM and HPF) differ in two ways (as explained in Section 2): a) the method of gathering the data, and b) the method of updating the grid.

Both map-building systems were evaluated within the obstacle set-ups shown in Fig. 2. The objects in Fig. 2a are cardboard boxes, Styrofoam partitions, and a 3/4 inch diameter cardboard pole; the single object in Fig. 2b is a box. The location of these objects was measured from a random starting position S. At the beginning of each run, the robot was accurately positioned at S.

4.2 Test Results

We first tested the HIMM method. Since this method is an integral part of our obstacle avoidance algorithm [4], only the target position needed to be specified for a run. The algorithm autonomously steers the robot among the obstacles on a smooth, continuous path (shown in grid resolution in Fig. 3). This procedure was performed ten times for each of the two obstacle courses in Fig. 2, and IOP measurements were recorded for each run.

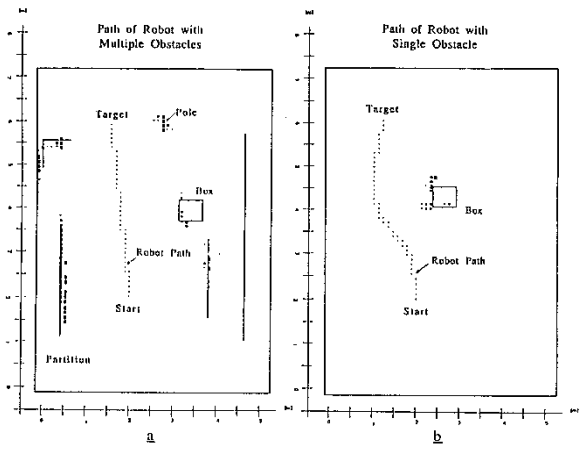

Fig 3. Paths of robot under control of the HIMM algorithm among multiple and single obstacle environments in grid resolution.

Next, the HPF algorithm was applied to the sensor readings taken by the robot at different locations. To produce similar conditions for this test, the locations were chosen along the continuous path defined by the HIMM run.

Again ten runs per obstacle environment (Fig 2a, b) were made, each one with 4 well-spaced locations on the path. Fig. 4 shows an example of a resulting map along with the robot positions from which the sensor data were taken. Results of all runs are summarized in Table 1.

Table 1.

Algorithm	Multiple Obstacles		Single Obstacle	
	$\overline{IOP}$	s	$\overline{IOP}$	s
HIMM	86.95	16.14	85.14	17.52
HPF	224.164	25.75	216.37	38.99

Summary of the Index of Performance statistic for runs using two different grid building algorithms. Ten runs were compiled for each algorithm. Statistics shown are the mean IOP ($\overline{IOP}$) and the standard deviations (s).

4.3 Discussion

The results demonstrate some of the important characteristics of the IOP. The mean IOP ($\overline{IOP}$) stays consistent regardless of obstacle environment. (86.95 and 85.14 for the HIMM and 224.16 and 216.37 for the HPF). This allows for comparison of algorithms originating from different labs using different obstacles and configurations.

The IOP also gives a quantitative measure of the differences in the sensor grid maps produced by each algorithm type. This difference can be visually identified in Fig. 4. Fig. 4a shows the result of a HPF run whereas Fig. 4b shows the result of a HIMM run.

The small black rectangles (blobs) represent filled sensor grid cells. Empty cells are not indicated. Each cell represents a real-world square of size 10cm *10cm. On the computer screen, CVs are coded with a different color for each one of the 16 possible CVs (ranging from 0 to 15). This effect cannot be reproduced in the screen-dumps of Fig. 4, but classes of low, medium, and high CVs can be distinguished by different blob sizes, as described in Fig. 4.

Both algorithms result in a fairly good representation of the obstacles (superimposed as solid lines in Fig. 4). The HPF has characteristic "arcs" corresponding to the distribution of values over all cells of the sensor cone at distance d (area A in Fig. 1a). This is especially evident in the representation of the pole (Fig. 4a). In general, there is a greater dispersion of sensor points about the obstacles as compared with the HIMM algorithm (Fig. 4b). This dispersion is measured by the IOP. The computed IOP value of 220 for the HPF means that the average distance from any of the sensor grid entries to the obstacles is about 220mm or about 2 grid cells (10cm by 10cm each in our case). The minimal dispersion of sensor entries for the HIMM method (Fig. 4b) results in an average of under 1 grid cell (86mm).

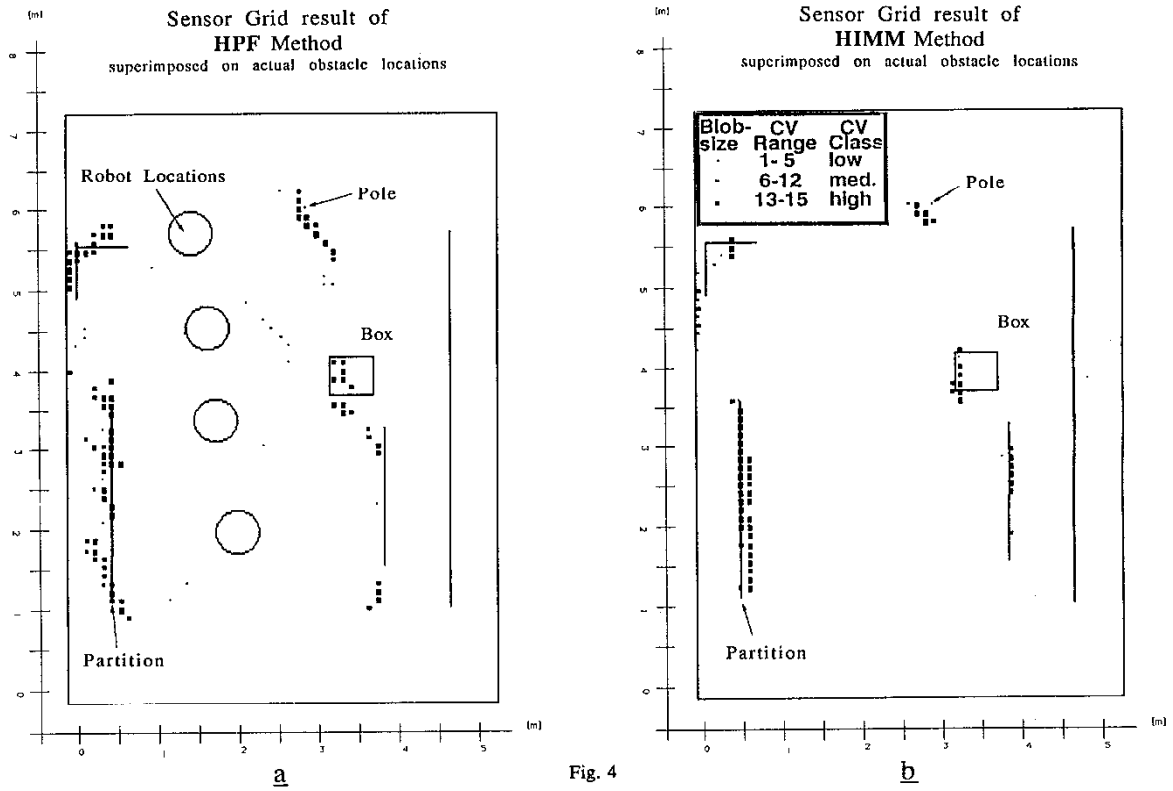

a b

Fig. 4

a) Sensor grid result using the heuristic probability function (HPF) algorithm.
b) Sensor grid result using the Histogramic In-Motion Mapping (HIMM) algorithm.

5. Conclusion

The proposed IOP was used to analyze the quality of two different map building methods. The HIMM method resulted in a sensor grid with entries in close proximity to actual object locations. This resulted in a favorable (low) IOP value. In contrast, the grid update rules and probability distribution functions used in the HPF method produced a sensor grid with a larger number of sensor grid entries further from actual object locations. Although these were often of low certainty value (CV), they resulted in a larger index of performance (IOP) value indicating a less precise representation of the actual environment.

The IOP can be used to analyze different methods of grid type map building. The simple quantitative representation of the IOP allows the investigator to comprehend the quality of the maps easily since the value is expressed in measurement units.

The IOP tool is used in the authors' lab to measure various map building and sensor grid enhancement routines as well as the effect of parameter modifications within these routines. The straightforward visualization of the IOP gives reason to expect that this measure will serve a versatile role in future map building research.

References

1. Beckerman M. and Oblow, E. M., "Treatment of Systematic Errors in the Processing of Wide Angle Sonar Sensor Data for Robotic Navigation." Accepted for publication in the *IEEE Journal of Robotics and Automation*, 1989.

2. Borenstein, J. and Koren, Y., "Obstacle Avoidance With Ultrasonic Sensors." *IEEE Journal of Robotics and Automation*, Vol. RA-4, No. 2, 1988, pp. 213-218.

3. Borenstein, J. and Koren, Y., "Real-time Obstacle Avoidance for Fast Mobile Robots." *IEEE Transactions on Systems, Man, and Cybernetics*, vol. 19, no 6, September 1989.

4. Borenstein, J. and Koren, Y., "Histogramic In-motion Mapping for Mobile Robot Obstacle Avoidance." Submitted for publication in the *IEEE Journal of Robotics and Automation*, September 1989.

5. Borenstein, J. and Koren, Y., "Real-time Obstacle Avoidance for Fast Mobile Robots in Cluttered Environments." To be presented at the 1990 *IEEE International Conference on Robotics and Automation*, Cincinnati, Ohio, May 13-18, 1990.

6. Borenstein, J. and Koren, Y., "The Vector Field Histogram - Fast Obstacle Avoidance for Mobile Robots." Submitted for publication in the *IEEE Journal of Robotics and Automation*, July 1989.

7. Brooks, R. A., "A Robust Layered Control System for a Mobile Robot." *IEEE Journal of Robotics and Automation*, Vol. RA-2, No. 1, 1986, pp. 14-23.

8. Brooks, R. A. and Connell, J. H., "Asynchronous Distributed Control System for a Mobile Robot." Proceedings of the SPIE, Mobile Robots, Vol. 727, 1987, pp. 77-84.

9. Burks, B. L. et al., "Autonomous Navigation, Exploration, and Recognition Using the HERMIES-IIB Robot." *IEEE Expert*, Winter 1987, pp. 18-27.

10. Crowley, J. L., "World Modeling and Position Estimation for a Mobile Robot Using Ultrasonic Ranging." *Proceedings of the 1989 IEEE International Conference on Robotics and Automation*, Scottsdale, Arizona, May 14-19, 1989, pp. 674-680.

11. Flynn, A. M., "Combining Sonar and Infrared Sensors for Mobile Robot Navigation." *The International Journal of Robotics Research*, Vol. 7, No. 6, December 1988, pp. 5-14.

12. Korba, L. W., Liscano, R., and Durie, N., "An Intelligent Mobile Platform for Health Care Applications." *Proceedings of the ICAART 88 conference*, Montreal, Canada, 1988, pp. 462-463.

13. Kuc, R. and Barshan, B., "Navigating Vehicles Through an Unstructured Environment With Sonar." *Proceedings of the 1989 IEEE International Conference on Robotics and Automation*. Scottsdale, Arizona, May 14-19, 1989, pp. 1422-1426.

14. Moravec, H. P. and Elfes, A., "High Resolution Maps from Wide Angle Sonar." *Proceedings of the IEEE Conference on Robotics and Automation*, Washington, D.C., 1985, pp. 116-121.

15. Moravec, H. P., "Sensor Fusion in Certainty Grids for Mobile Robots." *AI Magazine*, Summer 1988, pp. 61-74.

16. Pin, F.G., Beckerman, M., et. al., "Autonomous Mobile Robot Research Using the Hermies-III Robot", Invited Paper for the 1989 *"IROS" International Conference on Intelligent Robot and Systems*, "The Autonomous Mobile Robot and Its Application", September 1989, Tsukuba, Japan.

17. POLAROID Corporation, Ultrasonic Components Group, 119 Windsor Street, Cambridge, Massachusetts 02139, 1989.

18. Weisbin, C. R., de Saussure, G., and Kammer, D., "SELFCONTROLLED. A Real-Time Expert System for an Autonomous Mobile Robot." Computers in Mechanical Engineering, September 1986, pp. 12-19.